Single Archimedean Spiral Close Packed Phased Array HIFU

Kyle P. Morrison, MSBME & George W. Keilman, MSEE
Sonic Concepts, Inc.
Bothell, United States of America
kmorrison@sonicconcepts.com

Peter J. Kaczkowski, Ph.D.
Verasonics, Inc.
Redmond, United States of America

***Abstract*—This paper describes a series of high intensity focused ultrasound (HIFU) phased array transducers with a single Archimedean spiral close packed element arrangement on a spherical surface extending from the central axis outward. Simulation and measurement reveal using the spiral element arrangement on a spherical bowl reduces grating side lobes while maximizing power density at the focus.**

Keywords—HIFU, transducer, grating, lobes, spiral

I. Introduction

Many constraints present themselves when designing therapeutic transducer arrays for tissue ablation, mechanical cavitation, histotripsy and radiation force applications. These constraints are defined upon acoustic requirements such as acoustic power density, steering range, operating band and conversion efficiency. This paper describes a transducer design over a range of configurations to fit within these design constraints, with an emphasis on reducing grating lobes within and outside the steering range.

Prior art in radio frequency and ultrasound describe random, pseudo-random and geometrically packed array systems to reduce the grating lobes and unwanted interferences outside of the intended peak signal. Further data suggests spiral patterns reduce grating lobes for similar reasons. Random arrays are not geometrically packed and therefore have a poor active-to-total-aperture ratio. Other array concepts use non-circular elements producing asymmetrical/non-axisymmetric single-channel beams and impose manufacturing challenges. Using a periodic arrangement such as a spiral for HIFU will reduce the grating lobes, maximize the active to total aperture area, utilize axisymmetric elements and carry over proportionally to other transducer configurations with different frequencies and number of elements.

II. Materials and Equipment

Several configurations within a series of transducers have been characterized using a fixed geometry and a range in frequency to fit within the operating limits of the Vantage Research Ultrasound System and HIFU External Power Supply from Verasonics, Inc. Although more frequency options are available beyond the operating limits of the Vantage System, this paper focuses on 1.1, 2.0 and 4.0 MHz and element arrangements 128, 256, 512 and 2048, for a total of 11 different configurations (2,048 elements x 1.1 MHz is not available).

The transducer series uses a stack design that maximizes the electrical to acoustic efficiency to 80% over a 40% bandwidth centered about the center frequency. The cable, circuit board and matching networks are designed to maximize the efficiency and bandwidth of the transducer while matching each individual driving channel to a 75 Ohm / 0 degree load impedance. The matching circuit network enclosure is designed to plug directly into the Verasonics system connectors.

The 128 element x 2 MHz transducer's pressure field (Sonic Concepts Model H-302) was measured using the Vantage 256 System from Verasonics without the HIFU External Power Supply and using the internal imaging power supply. A 0.5 mm diameter Precision Acoustics hydrophone was used to measure the pressure field in an anechoic degassed test tank. A Sonic Concepts RFB-102 force balance was used to measure the power density and operating band.

a. Element Arrangement

Each configuration within the aforementioned design uses a single Archimedean spiral arrangement normal to the spherical bowl. Element arrangements are comprised of circular elements sized to fill the available space of a spherical bowl with the following geometry: 15.0 cm outside diameter x 4.4 cm inside diameter x 15.0 cm radius of curvature (f/1.0). The average active to total aperture area is 60% over the series of transducers. The single Archimedean spiral starts at X=0, tangent to the inside diameter and travels in a tightly packed 3-dimensional spiral until its last element is tangent to the outside diameter. Fig. 1 displays the 128, 256, 512 and 2,048 element configurations respectively.

Fig. 1. 128 element (upper left), 256 element (upper right), 512 (lower left) & 2,048 element (lower right) configurations.

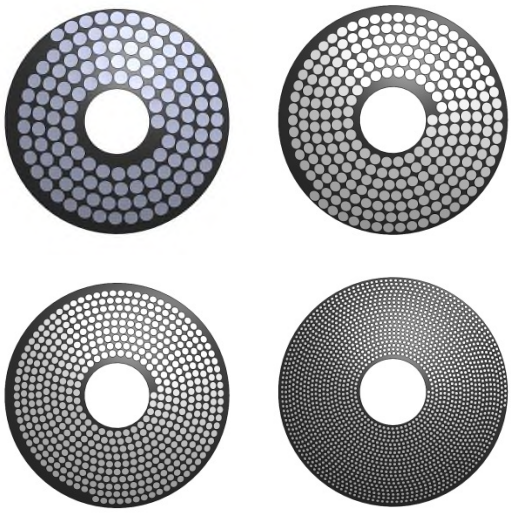

b. Simple Steering Calculations

Simple calculations were used to estimate the transverse and axial steering range for all 11 devices ignoring the element arrangement and overall size of the aperture. The lateral width of a single element at the focal plane is representative of the steering limit for any phased array. A Rayleigh-Sommerfeld integral program computes the lateral width for each configuration using the element's diameter and frequency.

Fig. 2 compares the lateral steering and peak amplitude on an absolute scale. Each transducer uses an average power RF input of 1,200 Watts, a calculated pressure gain assuming a free field and 80% electrical to acoustic efficiency.

Fig. 2. Linear scale lateral width simple calculations in a free field.

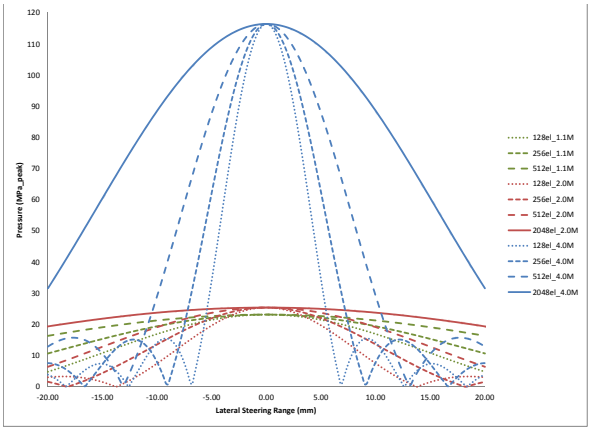

Fig. 3 below compares the simple calculated lateral steering ranges on a log scale. As expected, the 128el_1.1MHz, 512el_2.0MHz and 2048el_4.0MHz are coincident due to the consistent ratio of element diameter to wavelength.

Fig. 3. Normalized log scale lateral with simple calculations in a free field.

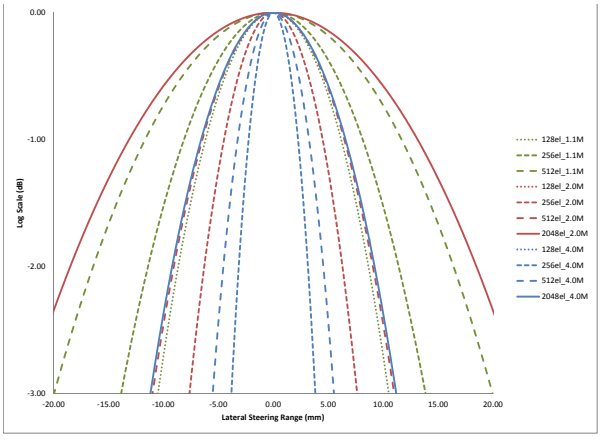

TABLE 1. LATERAL STEERING RANGE (IN MM).

Lateral Steering Range			
Number of Elements	Frequency		
	1.1 MHz	2 MHz	4 MHz
128	21.2	11.6	5.80
256	27.8	15.3	7.60
512	39.8	21.9	11.00
2048	NA	45.2	22.20

The simple calculation for axial steering range can be geometrically defined by using the two outermost elements of a transducer array. Superimposing the lateral width of each of the two outer elements located at the effective angle (or half of the total aperture area) creates an axial length approximation.

Fig. 4. Diagram used to geometry define the axial length.

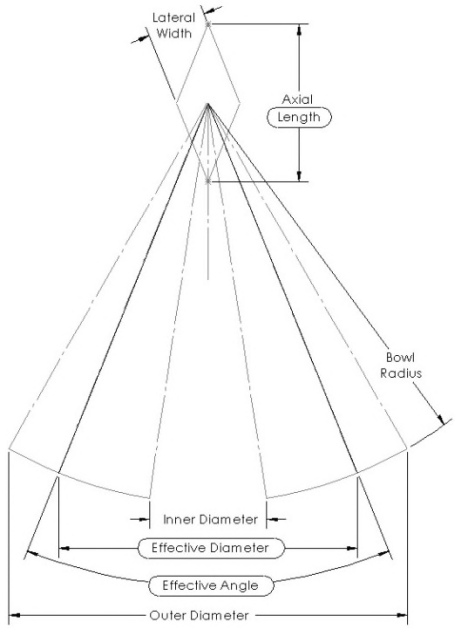

Known:

- Single Element Lateral Width
- Total Spherical Aperture Dimensions: Radius of Curvature (ROC), Outer Diameter (OD) & Inner Diameter (ID)

Solve:

- Effective Area = Total aperture / 2
- Height (h) = [ROC2 – (OD/2) 2]0.5 - [ROC2 – (ID/2) 2]^0.5
- Effective Diameter = Effective Area / (2πh)
- Effective Angle = 2 * Sine[(Effective Diameter / 2) / ROC]
- Constrain diamond geometry parallel to effective angle and calculate Axial Length

TABLE 2. AXIAL STEERING RANGE (IN MM).

Axial Steering Range			
Number of Elements	Frequency		
	1.1 MHz	2 MHz	4 MHz
128	56.6	31.0	15.48
256	66.2	40.8	20.28
512	106.2	58.5	29.36
2048	NA	120.6	59.25

An alternative approach to qualitatively define the axial length is to generate a point spread function with two elements from opposite sides, with maximum angle, with respect to the transducer spherical surface. Simulations were developed in coherent and incoherent format for the 128 element x 2 MHz configuration in plane and out of plane of the two elements.

Fig. 5. Two elements in-plane, incoherent estimate of steering boundaries.

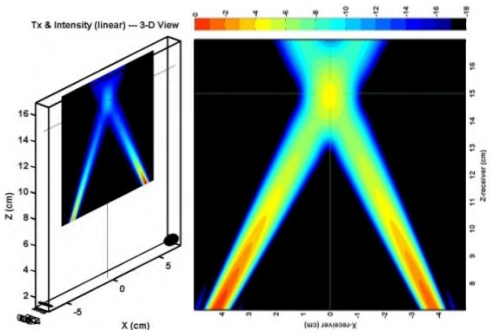

The in-plane incoherent results show a qualitative representative geometry of the steering range in the axial plane. Unfortunately these results do not present precise limits down -3 dB from peak output. Nevertheless, simply taking the intersection of a single element beam pattern with the array axis, for an element of "average position", leads to an excellent estimate of the steering range the array can achieve (see Fig. 7).

III. Array Simulation Results

To prove these simple calculations are acceptable approximations, three dimensional free field point spread function simulations were developed in coherent and incoherent format for the 128 element x 2 MHz configuration.

The 128 element array intensity beams are calculated at the focal plane from -20 mm to 20 mm in 1 mm increments along the X-axis. Fig. 6 below shows the normalized lateral width of a single element with a diameter of 10 mm from the 128 element array superimposed with the normalized beams calculated from the coherent sum of the array. The lateral width agrees with the steering range, and is assumed to carry over in principle to all configurations within the series under evaluation.

Fig. 6. Normalized intensity of single element lateral width (in cm) vs. 128 elements x 2 MHz lateral beam steering.

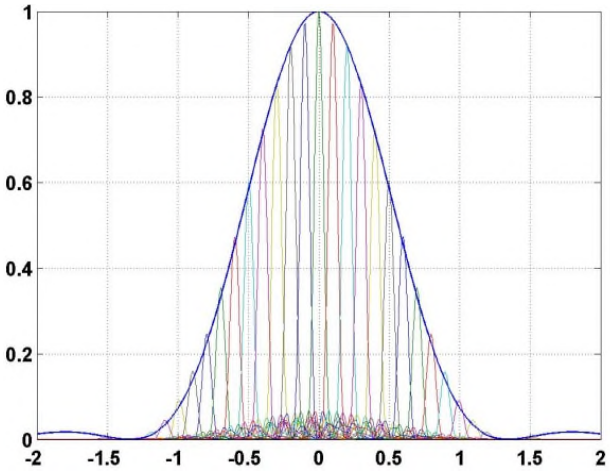

Fig. 7 presents the 128 element x 2 MHz array axial steering compared to a single element axial intercept of the "average position", or element 64 in this case. A spherical bowl with a 15.0 cm radius and 6.0 cm diameter (f/2.5) will also represent the "average area" for this series of transducers. The f/2.5 single element representation carries through the series of configurations as a constant, assuming 60% active to total aperture. Whereas using the element of "average position" can be used regardless of the active to total aperture ratio. The -3 dB falloff in the axial direction is in close agreement with the geometric simple calculation used earlier.

Fig. 7. Normalized intensity of single element axial intercept beam pattern vs. 128 elements x 2 MHz axial beam steering. The heavy blue line is the intesnity of the 64th element in the sprial, evaluated along the array axis.

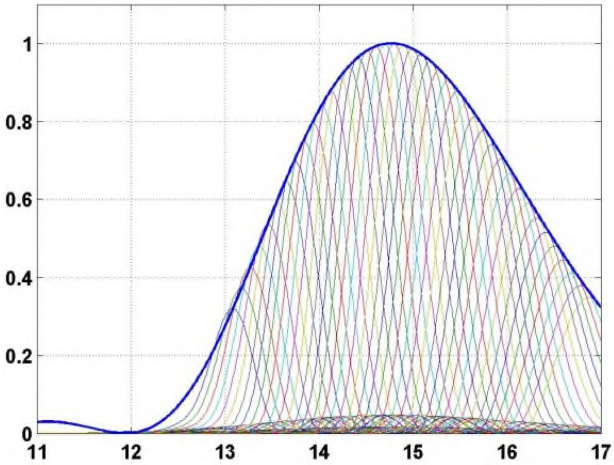

With respect to the ratio of the element diameter to wavelength the 128 element x 2 MHz is proportionate to the 512 elements x 4 MHz. Fig. 8 below displays the simulation results of the normalized intensity lateral and axial steering range for the 512 element x 4 MHz configuration using 5 mm diameter elements.

Fig. 8. 512 elements x 4 MHz, normalized intensity lateral (left) and axial (right), in cm.

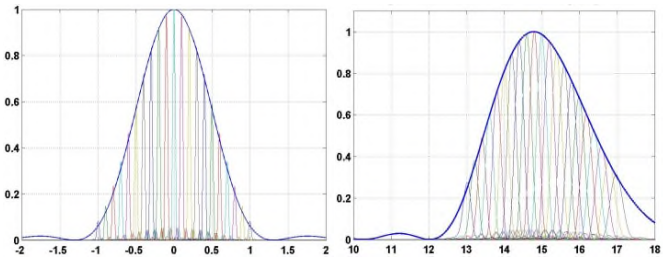

IV. Measurements

Pressure maps were primarily taken on H-302 SN: -067 to verify the acoustic output of the built device performs similarly to simulations of the 128 element x 2 MHz configuration. The geometric focus at the origin measured 0.80 mm in lateral width and 7.34 mm in axial length.

Fig. 9. Axial plane at Y=0 of geometric focus, in relative pressure.

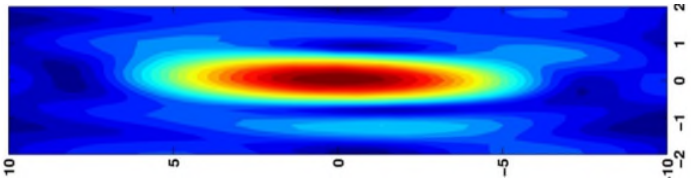

Fig. 10 below confirms the association between the calculated single element lateral width and the measured array lateral steering width.

Fig. 10. Normalized log scale measured lateral steering vs. calculated single element lateral width.

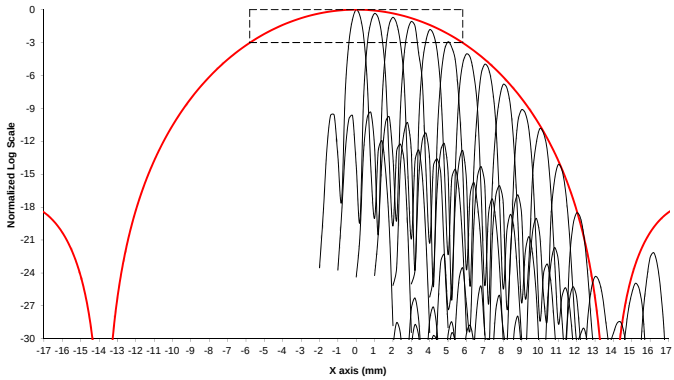

Fig. 11 below confirms the association between the calculated single element with the same ROC and f/2.5 axial length and the measured array axial steering length.

Fig. 11. Normalized log scale measured axial steering vs. calculated single element f/2.5 axial length.

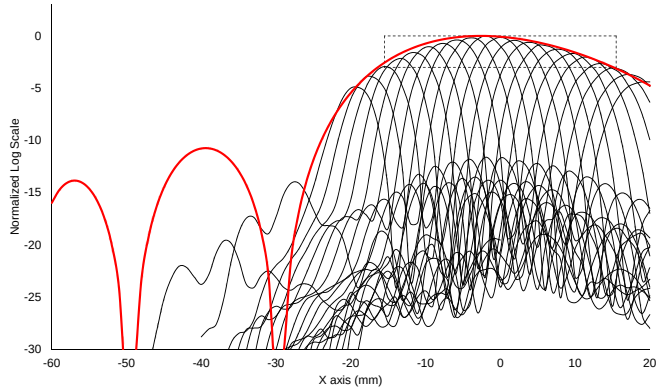

a. Non linearities

The Vantage 256 System was programmed to produce a 10 cycle burst at 1.6 Volt_pk into a 75 Ohm load, which correlates to an estimated 1.94 MPa_peak pressure at the geometric focus assuming a linear free field. The water path from the radiating surface to the focus and pressure behavior in the acoustic field adds to the non linear structure of the waveform. When -4 dB outside of the peak pressure, the non linearities subside, indicating that the non-linear behavior is mostly noticeable when pressure amplitudes are very high due to coherent focusing, and essentially negligible away from the focus and high intensity sidelobes.

Fig. 12. Waveform capture at origin (blue) vs. X = 8 mm off origin (red).

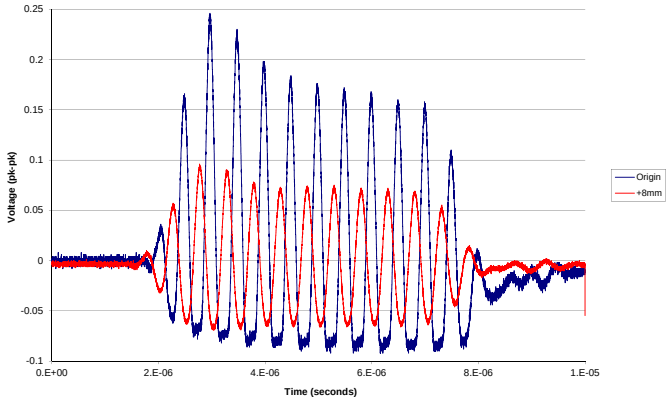

b. Grating Lobes

The paper thus far has presented the steering range based on the -3 dB fall off, or full-width-half-maximum intensity (FWHM intensity), in both the lateral and axial directions. An alternative expression of the steering range can be defined as the point where the grating lobes are within -3 dB of the intended focus.

Fig. 13 compares the measured transverse field (left) vs. simulation (right) on a normalized log scale.

Fig. 13. Normalized log scale measured (left) vs. simulated (right) transverse pressure field, focus X = 8 mm off origin.

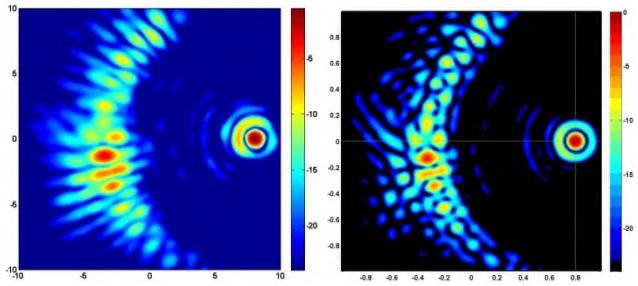

The focus is steered to X = 8 mm & Y, Z = 0 mm. This focus is outside of the +/- 5.8 mm in lateral width according to FWHM intensity. Although it is 2.2 mm past the FWHM, measurement proves the highest grating lobe is only reaching -6 dB. The full volumetric field indicates that this is the peak grating lobe for this example.

Fig. 14 compares the measured axial field (left) vs. simulation (right) on a normalized log scale. The focus is steered to X = 8 mm, Y = 5.8 mm and Z = 0 mm. Again, this point is outside of the FWHM range. The highest measured grating lobe appears -8 dB from the focus.

Fig. 14. Normalized log scale measured (left) vs. simulated (right) axial pressure field, focus X = 8 & Z = 5.8 mm off origin.

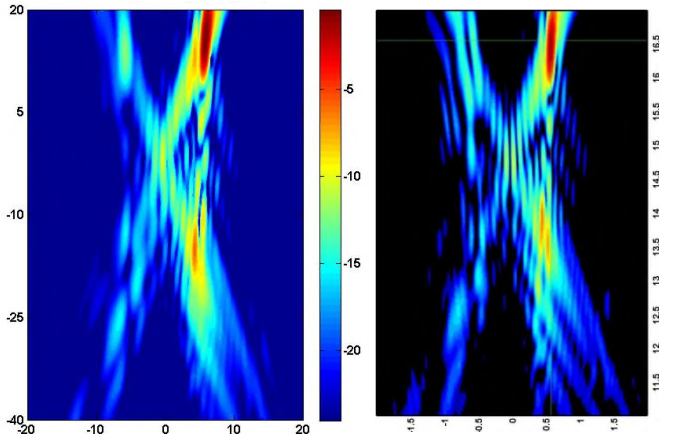

In using the 11.6 mm lateral width by 31 mm axial length to create an ellipsoidal volume, an arbitrary point can be chosen in 3-dimensions to measure the axial pressure field. In the case below we chose a point on the FWHM intensity surface of the ellipsoidal volume at X = 2.4 mm, Y = 2.5 mm & Z = 12. 4 mm. The highest grating lobe in this plane appears to be located -8 dB from the focus.

Fig. 15. Normalized log scale measured axial pressure field, focus X = 2.4, Y = 2.5 & Z = 12.4 mm off origin.

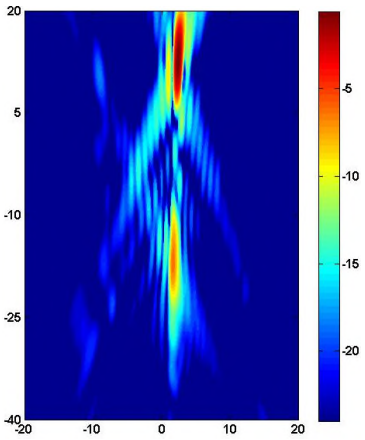

V. Conclusions

This work suggests that the Archimedean spiral arrangement is sufficient in minimizing grating lobes and maximizing power density for the described series of array transducers. Furthermore, simple calculations used to predict the FWHM intensity of an array are in good agreement using complex array point spread functions. The simple calculation rules and the Archimedean spiral pattern can be used across a wide range of designs, with reduced grating lobes in the near and far fields.

The usable steering range is somewhat larger than the conventional FWHM intensity volume. The steering range can extend outside the ellipsoidal volume to a boundary defined by focal points where the nearest grating lobe is within -3 dB.

References

[1] B. Raju, C. Hall and R. Seip, "Ultrasound Therapy Transducers With Space Filling Non-Periodic Arrays," IEEE Trans. Ultrason., Ferroelectr. Freq. Control, vol. 58, no. 5, pp. 944-954, May 2011.

[2] L. R. Gavrilov, J. W. Hand, P. Abel, and C. A. Cain, "A method of reducing grating lobes associated with an ultrasound linear phased array intended for transrectal thermotherapy," IEEE Trans. Ultrason., Ferroelectr. Freq. Control, vol. 44, no. 5, pp. 1010-1017, 1997.

[3] B. Gruendaum and G. C. Shephard, Tiling and Patterns. New York, NY: W. H. Freeman, 1987.

[4] M. Lu, M. Wan, F. Xu, X. Wang, and H. Zhong, "Focused beam control for ultrasound surgery with shpherical-section phased array and precise control of multi-focus patterns," Acta Physica Sinica, vol. 59, pp. 1349-1356, Feb. 2010.

[5] F. Dupenloup, J. Y. Chapelon, D. J. Cathignol, and O. A. Sapozhnikov, "Reduction of the grating lobes of annular arrays used in focused ultrasound surgery," IEEE Trans. Ultrason., Ferroelectr. Freq. Control, vol. 43, no. 6, pp. 991-998, 1996.